Available online at www.sciencedirect.com
ScienceDirect
Journal of Sound and Vibration 299 (2007) 520–539
JOURNAL OF SOUND AND VIBRATION
www.elsevier.com/locate/jsvi

Bifurcation analysis of a two-degree-of-freedom aeroelastic system with freeplay structural nonlinearity by a perturbation-incremental method

K.W. Chung[a,*], C.L. Chan[a], B.H.K. Lee[b]

[a]*Department of Mathematics, City University of Hong Kong, Tat Chee Avenue, Kowloon, Hong Kong*
[b]*Aerodynamics Laboratory, National Research Council, Institute for Aerospace Research, Ottawa, Ontario, Canada K1A 0R6*

Received 22 September 2005; received in revised form 9 June 2006; accepted 19 June 2006
Available online 4 October 2006

Abstract

A perturbation-incremental (PI) method is presented for the computation, continuation and bifurcation analysis of limit cycle oscillations (LCO) of a two-degree-of-freedom aeroelastic system containing a freeplay structural nonlinearity. Both stable and unstable LCOs can be calculated to any desired degree of accuracy and their stabilities are determined by the Floquet theory. Thus, the present method is capable of detecting complex aeroelastic responses such as periodic motion with harmonics, period-doubling (PD), saddle-node bifurcation, Neimark–Sacker bifurcation and the coexistence of limit cycles. Emanating branch from a PD bifurcation can be constructed. This method can also be applied to any piecewise linear systems.

1. Introduction

The study of the dynamic behaviour of aircraft structures is crucial in flutter analysis since it provides useful information in the design of aircraft wings and control surfaces. Concentrated structural nonlinearities can have significant effects on the aeroelastic responses of aerosurfaces even for small vibrational amplitudes. One particular concentrated structural nonlinearity that has received much attention is the bilinear or freeplay spring, which is a representative of worn or loose control surface hinges.

A freeplay nonlinearity in pitch was first studied by Woolston et al. [1] and Shen [2]. They showed that limit cycle oscillation (LCO) might occur well below the linear flutter boundary. McIntosh et al. [3] performed experimental work with a wind tunnel model having two degrees of freedom (dof). They found that the behaviour of the airfoil was extremely dependent on the initial pitch deflection. Yang and Zhao [4] considered LCO of a two-dimensional airfoil in incompressible flow using the Theodorsen function. Two stable LCOs of different amplitudes were detected for some airspeeds. Hauenstein et al. [5] investigated theoretically and experimentally a rigid wing flexibly mounted at its root with freeplay nonlinearities in both pitch and plunge

*Corresponding author. Tel.: +852 27888671; fax: +852 27888561.
E-mail address: makchung@cityu.edu.hk (K.W. Chung).

0022-460X/$ - see front matter
doi:10.1016/j.jsv.2006.06.059

degrees of freedom. They obtained excellent agreement between theoretical and experimental results, and concluded that chaotic motion did not occur with a single root nonlinearity. However, Price et al. [6,7] pointed out that such conclusion was not true. Tang and Dowell [8] analysed the flutter instability and forced response of a helicopter blade wind-tunnel model with no rotation. For a narrow range of airspeeds, the system exhibited both LCO and chaotic behaviour. Kim and Lee [9] investigated the dynamics of a flexible airfoil with a freeplay nonlinearity. They observed that LCO and chaotic motions were highly influenced by the pitch–plunge frequency ratio.

An aeroelastic model with freeplay nonlinearity has been investigated using analytical methods based on describing function and harmonic balance methods. By using the incremental harmonic balance (IHB) method, Lau and Zhang [10] studied nonlinear vibrations of piecewise-linear systems in which the freeplay nonlinearity is a special case. The main drawback of using harmonic balance methods to investigate freeplay nonlinearity is that the second derivative of an approximate solution obtained by such methods is continuous while that of the exact solution is discontinuous at the switching points where changes in linear subdomains occur. Such inconsistency between the exact and approximate solutions may lead to serious error in the prediction and analysis. To overcome this drawback, Liu et al. [11] introduced the point transformation (PT) method which could track the system behaviour to the exact point where the change in linear subdomains occurred. Moreover, complex nonlinear aeroelastic behaviour such as periodic motion with harmonics, periodic doubling, chaotic motion and the coexistence of stable limit cycles can be detected. However, The PT method is not capable of finding unstable periodic solutions and thus is not suitable for performing parametric continuation.

Recently, Chan et al. [12] presented a perturbation-incremental (PI) method for the study of limit cycles and bifurcation analysis of strongly nonlinear autonomous oscillators with arbitrary large bifurcation values. The PI method is a semi-analytical and numerical process which incorporates salient features from both the perturbation method and the incremental approach. This method was later extended to investigate coupled nonlinear oscillators [13,14] and delay differential equations [15].

In this paper, we extend the PI method to the continuation and bifurcation analysis of an aeroelastic model with freeplay nonlinearity. In fact, the method can also be applied to any piecewise-linear system. Both stable and unstable periodic solutions can be calculated and their stabilities are determined by using the Floquet theory. The paper is organized as follows. A brief description of an aeroelastic model with freeplay nonlinearity is given in Section 2. The PI method is described in Section 3. Section 4 deals with the computation of stability of a LCO. Bifurcation analysis is considered in Section 5, followed by conclusions in Section 6 and two appendices.

2. The mathematical model

Fig. 1 shows a sketch of a 2 dof airfoil motion in plunge and pitch. The plunge deflection is denoted by h, positive in the downward direction, and α is the pitch angle about the elastic axis, positive nose up. The elastic axis is located at a distance $a_h b$ from the mid-chord, while the mass centre is located at a distance $x_a b$ from the elastic axis, where b is the airfoil semi-chord. Both distances are positive when measured towards the trailing edge of the airfoil. The aeroelastic equations of motion for linear springs have been derived by Fung [16]. For nonlinear restoring forces, the coupled bending-torsion equations for the airfoil can be written as follows:

$$m\ddot{h} + S\ddot{\alpha} + C_h\dot{h} + \bar{G}(h) = p(t), \tag{1}$$

$$S\ddot{h} + I_\alpha\ddot{\alpha} + C_\alpha\dot{\alpha} + \bar{M}(\alpha) = r(t), \tag{2}$$

where the symbols m, S, C_h, I_α and C_α are the airfoil mass, airfoil static moment about the elastic axis, damping coefficient in plunge, wing mass moment of inertia about elastic axis, and torsion damping coefficient, respectively. $\bar{G}(h)$ and $\bar{M}(\alpha)$ are the nonlinear plunge and pitch stiffness terms, and $p(t)$ and $r(t)$ are the forces and moments acting on the airfoil, respectively. By a suitable transformation as described in Refs. [11,17,18], the two-dimensional airfoil motion without any external forces can be rewritten into a system of

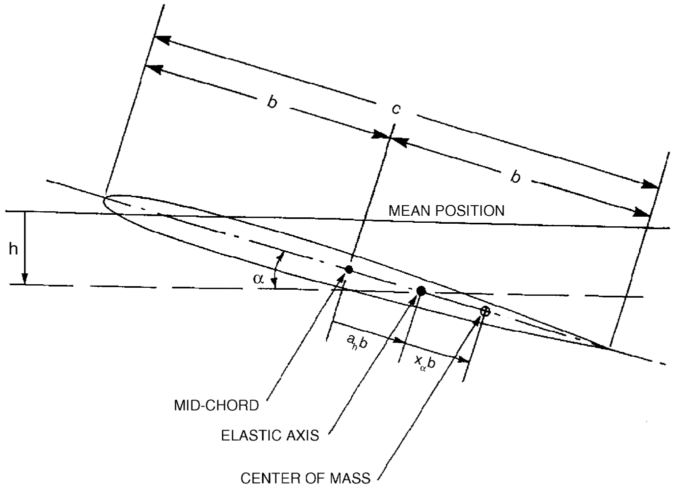

Fig. 1. Schematic of airfoil with 2 dof motion.

eight first-order ordinary differential equations

$$
\begin{aligned}
x_1' &= x_2,\\
x_2' &= a_{21}x_1 + a_{22}x_2 + a_{23}x_3 + a_{24}x_4 + a_{25}x_5 + a_{26}x_6 + a_{27}x_7\\
&\quad + a_{28}x_8 + j\left(d_0\left(\frac{\bar{\omega}}{U^*}\right)^2 G(x_3) - c_0\left(\frac{1}{U^*}\right)^2 M(x_1)\right),\\
x_3' &= x_4,\\
x_4' &= a_{41}x_1 + a_{42}x_2 + a_{43}x_3 + a_{44}x_4 + a_{45}x_5 + a_{46}x_6 + a_{47}x_7\\
&\quad + a_{48}x_8 + j\left(c_1\left(\frac{1}{U^*}\right)^2 M(x_1) - d_1\left(\frac{\bar{\omega}}{U^*}\right)^2 G(x_3)\right),\\
x_5' &= x_1 - \varepsilon_1 x_5,\\
x_6' &= x_1 - \varepsilon_2 x_6,\\
x_7' &= x_3 - \varepsilon_1 x_7,\\
x_8' &= x_3 - \varepsilon_2 x_8,
\end{aligned}
\tag{3}
$$

where the $'$ denotes differentiation with respect to the non-dimensional time τ defined as $\tau = Ut/b$ with U being the free-stream velocity. The coefficients j, $a_{21}, \ldots, a_{28}$, $a_{41}, \ldots, a_{48}$, c_0, c_1, d_0, d_1, ε_1 and ε_2 are related to the system parameters and their expressions are given in Appendix A. The structural nonlinearities are represented by the nonlinear functions $G(x_3)$ and $M(x_1)$. In this paper, we investigate system (3) for a freeplay spring in pitch and a linear spring in plunge, where $M(x_1)$ is given by

$$
M(x_1) = \begin{cases} M_0 + x_1 - \alpha_f, & x_1 < \alpha_f,\\ M_0 + M_f(x_1 - \alpha_f), & \alpha_f \leqslant x_1 \leqslant \alpha_f + \delta,\\ M_0 + x_1 - \alpha_f + \delta(M_f - 1), & x_1 > \alpha_f + \delta, \end{cases}
\tag{4}
$$

where M_0, M_f, α_f and δ are constants, and $G(x_3) = x_3$. A sketch of the freeplay model is given in Fig. 2.

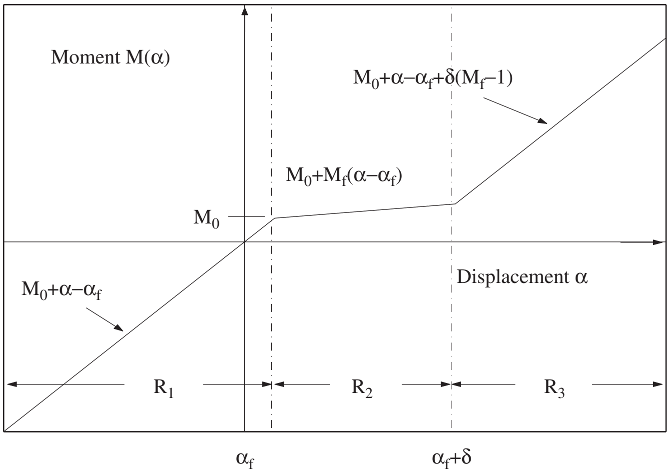

Fig. 2. General sketch of a freeplay stiffness.

According to the three linear branches of the bilinear function for a freeplay model, the phase space $X \in R^8$ can be divided into three regions, $R_i (i = 1, 2, 3)$, where each corresponds to a linear system:

$$X' = AX + F_1 \quad \text{in } R_1 = \{X \in R^8 | x_1 < \alpha_f\}, \tag{5a}$$

$$X' = BX + F_2 \quad \text{in } R_2 = \{X \in R^8 | \alpha_f < x_1 < \alpha_f + \delta\}, \tag{5b}$$

$$X' = AX + F_3 \quad \text{in } R_3 = \{X \in R^8 | x_1 > \alpha_f + \delta\}. \tag{5c}$$

The elements of A, B and $F_i (i = 1, 2, 3)$ are determined by the system parameters of the coupled aeroelastic equations, and they are given by

$$A = \begin{pmatrix} A_1 & A_2 \\ A_3 & A_4 \end{pmatrix}, \quad B = \begin{pmatrix} B_1 & A_2 \\ A_3 & A_4 \end{pmatrix} \tag{6}$$

and $F_1 = (M_0 - \alpha_f)F$, $F_2 = (M_0 - M_f \alpha_f)F$, $F_3 = (M_0 - \alpha_f + \delta_0(M_f - 1))F$ where $A_i (i = 1, 2, 3, 4)$, B_1 and the vector F are defined in Appendix B with $\beta = 1$.

Stable LCOs were obtained by using the PT method as described in Ref. [11]. In the subsequent sections, we apply the PI method to obtain both stable and unstable LCO and perform parametric continuation.

3. The PI method

In our previous studies of dynamical systems [12–15], the PI method was applied to smooth nonlinear systems. In the present paper, we extend the PI method to piecewise-linear systems.

Consider the freeplay model shown in Fig. 2. Let the Z–Y plane represent the eight-dimensional phase space, where $Z = \{x_1\}$ and $Y = \{x_2, x_3, x_4, x_5, x_6, x_7, x_8\}$. Let Z_1 and Z_2 denote the switching subspaces $Z = \alpha_f$ and $Z = \alpha_f + \delta$, respectively, where the linear systems change. The Z–Y phase space is now divided by Z_1 and Z_2 into three regions R_1, R_2 and R_3 as shown in Fig. 3(a). The system response can then be predicted by following a general phase path. Assuming that a motion initially starts at a point X_1 in one of the switching subspaces (say Z_1) as shown in Fig. 3(a), the trajectory passes through R_2, hits Z_2 at X_2 and enters into R_3. Then, it returns to R_2 through X_3 in Z_2 and hits Z_1 at X_4. It enters into R_1 and hits Z_1 again at X_5. The points $X_i, (i = 1, 2, 3, 4, 5)$ are called *switching points* as they are located in the switching subspaces. Let t_1 be the travelling time of the trajectory from X_1 to X_2 in region R_2. Similarly, let t_2, t_3 and t_4 be the travelling times of the trajectory in regionsR_3, R_2 and R_1, respectively. We note that the points X_1 and X_5 define a Poincaré map in Z_1. The trajectory becomes a LCO if X_1 coincides with X_5 (see Fig. 3(b)). Since the system of equations in

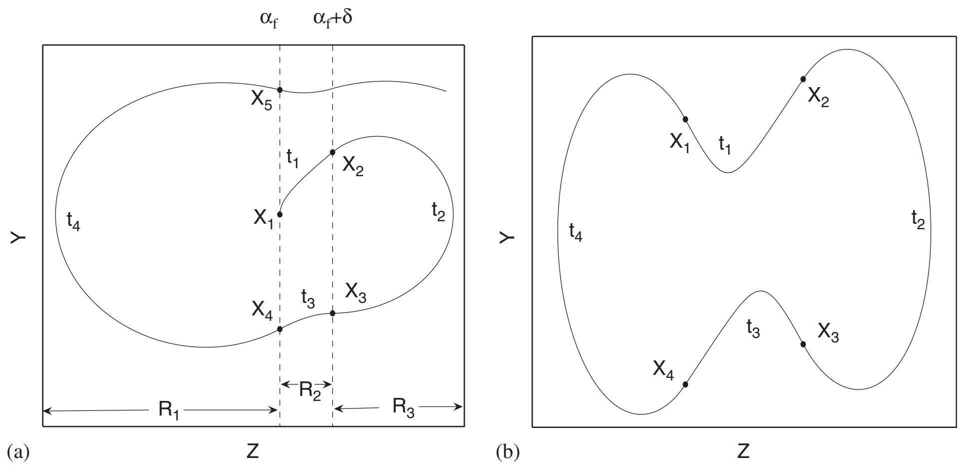

Fig. 3. General trajectory (a) and a period-one trajectory (b) of system (10) with a freeplay stiffness in pitch.

each region is strictly linear, the exact solutions in R_1, R_2 and R_3 can be expressed analytically. Therefore, for a given point X_1 in Z_1, X_5 can be determined analytically.

The main idea of the PI method is to convert a LCO to an equilibrium point of a Poincaré map in a switching subspace and consider a system of variational equations of the map for parametric continuation. Same as in Refs. [7,11], the non-dimensional velocity U^* is used as the bifurcation parameter.

The procedure of the PI method is divided into two steps. The first step is to obtain an initial solution for the continuation of the bifurcation parameter in the second step.

3.1. Perturbation step

For a smooth dynamical system, small LCO can be obtained through Hopf bifurcation. However, Hopf bifurcation theorems cannot be applied to a piecewise-linear system due to its low differentiability. Nevertheless, a piecewise-linear system can undergo bifurcations which have similarities (but also discrepancies) with the Hopf bifurcation [20]. Limit cycle bifurcation from centre in symmetric piecewise-linear systems was investigated in Ref. [21]. A system of the form $\dot{X} = F(X)$, $X \in R^n$ is *symmetric* if it satisfies the condition $F(-X) = -F(X)$. In fact, system (3) with structural nonlinearities defined in Eq. (4) is a symmetric piecewise-linear system. A LCO is *symmetric* if $X(t+T/2) = -X(t)$ where T is the period. An initial symmetric LCO may be obtained in the following way.

Assume that a pair of eigenvalues of the system in region R_2 become pure imaginary (say $\lambda = \pm \mathrm{i}\omega, \omega > 0$) at a specific value of the bifurcation parameter U^* and $\underset{\sim 1}{u} \pm \mathrm{i}\underset{\sim 2}{u}$ are the corresponding eigenvectors. A periodic solution in the linear subspace spanned by $\underset{\sim 1}{u}$ and $\underset{\sim 2}{u}$ can be expressed as

$$\begin{aligned} \underset{\sim}{r}(t) &= p'\mathrm{e}^{\mathrm{i}\omega t}(\underset{\sim 1}{u} + \mathrm{i}\underset{\sim 2}{u}) + \bar{p}'\mathrm{e}^{-\mathrm{i}\omega t}(\underset{\sim 1}{u} - \mathrm{i}\underset{\sim 2}{u}) + \underset{\sim 0}{u} \\ &= (p_1\cos\omega t - p_2\sin\omega t)\underset{\sim 1}{u} - (p_2\cos\omega t + p_1\sin\omega t)\underset{\sim 2}{u} + \underset{\sim 0}{u}, \end{aligned} \tag{7}$$

where $p_1 = (p' + \bar{p}')/2 \in R$, $p_2 = (p' - \bar{p}')/2i \in R$ and $\underset{\sim 0}{u} \in R^8$. Since $\underset{\sim}{r}(t)$ lies in region R_2, it follows from Eq. (5b) that

$$\underset{\sim 0}{u} = \begin{cases} -B^{-1}F_2 & \text{if } \det(B) \neq 0, \\ 0 & \text{if } \det(B) = 0 \text{ and } F_2 = \underset{\sim}{0}. \end{cases} \tag{8}$$

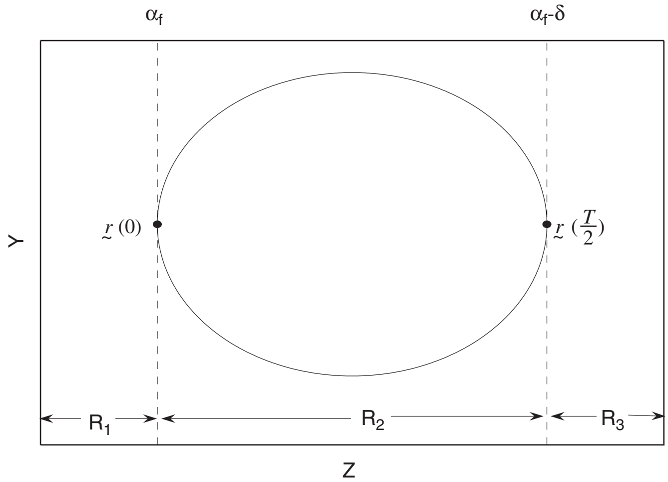

Fig. 4. Periodic solution with maximal amplitude in the linear subspace spanned by $\underset{\sim 1}{u}$ and $\underset{\sim 2}{u}$.

The system parameters considered in Refs. [7,11] and Section 5 have the condition that $F_2 = \underset{\sim}{0}$. The case that $\det(B) = 0$ and F_2 is nonzero will be discussed in Ref. [19]. If the linear subspace spanned by $\underset{\sim 1}{u}$ and $\underset{\sim 2}{u}$ intersects both the switching subspaces Z_1 and Z_2, then there exists a unique periodic solution touching both Z_1 and Z_2 with maximal amplitude. Assume that, at $t = 0$, $\underset{\sim}{r}(0)$ is the switching point at Z_1 (see Fig. 4). Then, $\underset{\sim}{r}(T/2)$ is the switching point at Z_2 where T is the period. It follows from Eq. (7) that

$$\begin{cases} \alpha_f = p_1 u_{11} - p_2 u_{21} + u_{01}, \\ \alpha_f + \delta = -p_1 u_{11} + p_2 u_{21} + u_{01}, \end{cases}$$
$$\Longrightarrow \begin{cases} p_1 u_{11} - p_2 u_{21} = -\delta/2, \\ u_{01} = \alpha_f + \delta/2, \end{cases} \tag{9a, b}$$

where u_{i1} $(i = 0, 1, 2)$ is the first component of $\underset{\sim i}{u}$. Since the tangents at the switching points are orthogonal to the Z-axis, the first component of $\underset{\sim}{\dot{r}}(0)$ is zero. Therefore, we have, from Eq. (7),

$$p_1 u_{21} + p_2 u_{11} = 0. \tag{10}$$

From Eqs. (9a,b) and (10), we obtain

$$p_1 = \frac{-\delta u_{11}}{2(u_{11}^2 + u_{21}^2)} \quad \text{and} \quad p_2 = \frac{\delta u_{21}}{2(u_{11}^2 + u_{21}^2)}. \tag{11}$$

The periodic solution with maximal amplitude can be uniquely determined from Eqs. (8), (9a,b) and (11). As the bifurcation parameter is varied from the critical value, a symmetric LCO traversing all three regions $R_i (i = 1, 2, 3)$ may suddenly appear.

This step gives the location of the switching points and travelling time of an initial LCO, which will be used in the incremental step.

3.2. Parameter incremental method—a Newton–Raphson procedure

To investigate the continuation in U^*, we note that, for a general LCO traversing all three regions, the number of switching points is not restricted to four. For example, the LCO in Fig. 5(a) contains six switching points. The complete loop covering the entire region also contains a smaller loop, covering the two regions R_1 and R_2. A complete loop is classified as a period-m LCO if it covers the entire region m times. Although the

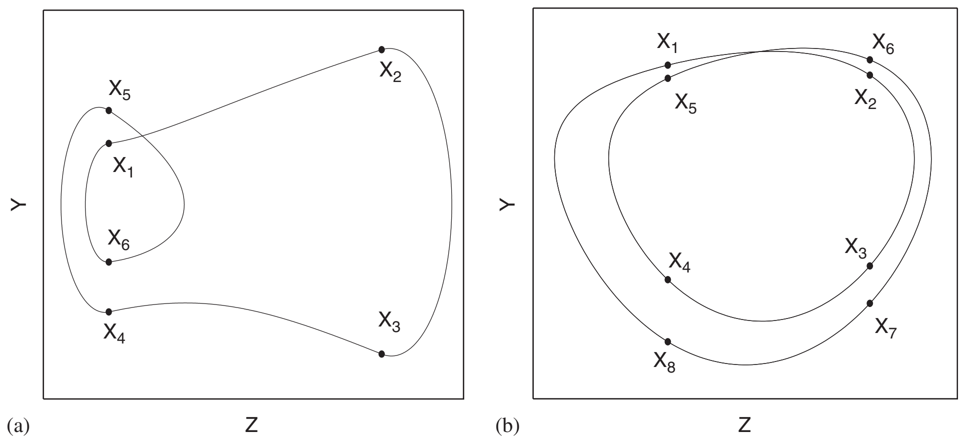

Fig. 5. The LCOs contain (a) six and (b) eight switching points.

LCO of Fig. 5(a) is of period-one, the presence of a smaller loop indicates that it has a harmonic component. In the subsequent sections, p-n-h denotes a period-n LCO with harmonics. In Fig. 5(b), the LCO contains eight switching points and is of period-two.

Assume that a LCO contains n switching points $X_i (1 \leqslant i \leqslant n)$. Let $\underset{\sim i}{r}(t)(1 \leqslant i \leqslant n)$ be the segment of LCO between the switching points X_i and X_{i+1} with $X_{n+1} = X_1$ and lie in the region $R_{p_i} (p_i \in \{1, 2, 3\})$. Let $\lambda_{hj} (j = 1, 2, \ldots, 8)$ and $\underset{\sim hj}{v}$ be the eigenvalues and eigenvectors, respectively, of the 8×8 matrices A if $h = 1, 3$ and B if $h = 2$. Then, $\underset{\sim i}{r}(t)$ can be expressed analytically as

$$\underset{\sim i}{r}(t) = \underset{\sim p_i 0}{v} + \sum_{j=1}^{8} k_{ij} \mathrm{e}^{\lambda_{p_i j} t} \underset{\sim p_i j}{v}, \quad 1 \leqslant i \leqslant n, \tag{12}$$

where $k_{ij} \in R$ and $\underset{\sim p_i j}{v} \in R^8$. To simplify the calculation, the time t in $\underset{\sim i}{r}(t)$ is defined in such a way that it counts only the time travelled in region R_{p_i}. Since $\underset{\sim i}{r}(t)$ is the trajectory from X_i to $X_{i+1} (X_{n+1} = X_1)$ with travelling time t_i, we have

$$X_i = \underset{\sim i}{r}(0) = \underset{\sim i-1}{r}(t_{i-1}), \quad 1 \leqslant i \leqslant n, \tag{13}$$

with subscript '0' replaced by 'n' (i.e. $\underset{\sim 0}{r}(t_0) = \underset{\sim n}{r}(t_n)$). This replacement of subscript '0' by 'n' will also be used in subsequent formulae derived from Eq. (13). Substituting Eq. (12) into Eq. (5), we obtain

$$\underset{\sim p_i 0}{v} = -C_{p_i}^{-1} F_{p_i}, \quad 1 \leqslant i \leqslant n, \tag{14}$$

where

$$C_{p_i} = \begin{cases} A & \text{if } p_i = 1, 3, \\ B & \text{if } p_i = 2. \end{cases}$$

Furthermore, substituting Eqs. (12) and (14) into Eq. (13), we obtain

$$X_i = \sum_{j=1}^{8} k_{ij} \underset{\sim p_i j}{v} - C_{p_i}^{-1} F_{p_i} = \sum_{j=1}^{8} k_{i-1 j} \mathrm{e}^{\lambda_{p_{i-1} j} t_{i-1}} \underset{\sim p_{i-1} j}{v} - C_{p_{i-1}}^{-1} F_{p_{i-1}}, \quad 1 \leqslant i \leqslant n. \tag{15}$$

The period of a LCO is given by $T = \sum_{i=1}^{n} t_i$. Let X_i be expressed as

$$X_i = \begin{pmatrix} \alpha_i \\ \underset{\sim i}{s}^* \end{pmatrix} \quad \text{where } \alpha_i = \begin{cases} \alpha_f & \text{if } X_i \in Z_1, \\ \alpha_f + \delta & \text{if } X_i \in Z_2, \end{cases} \text{ and } \underset{\sim i}{s}^* \in R^7. \tag{16}$$

If the system parameters such as a_{ij}, U^* in Eq. (3) are given, the matrices A, B are determined and, thus, the eigenvalues λ_{ij}, eigenvectors $\underset{\sim ij}{v}$ in Eq. (15) can be found. For a general LCO satisfying Eq. (15), assume that the switching subspaces in which X_is lie are all given, i.e. α_is are given for $1 \leqslant i \leqslant n$. The LCO can be determined by solving the $8 \times 2 \times n = 16n$ equations in Eq. (15) with the unknowns k_{ij} ($8n$ of them), $\underset{\sim i}{s}^*$ ($7n$) and t_i (n) where $1 \leqslant i \leqslant n$ and $1 \leqslant j \leqslant 8$. If one of the switching points (say X_1) is given, the complete loop including all the other switching points and its period can be determined from Eq. (15). To consider the continuation in U^*, a small increment of U^* to $U^* + \Delta U^*$ in Eq. (15) corresponds to small changes of the following quantities

$$k_{ij} \to k_{ij} + \Delta k_{ij}, \quad \underset{\sim i}{s}^* \to \underset{\sim i}{s}^* + \Delta \underset{\sim i}{s}^* \text{ and } t_i \to t_i + \Delta t_i.$$

To obtain a neighbouring solution, Eq. (15) are expanded in Taylor's series about an initial solution and linearized incremental equations are derived by ignoring all the nonlinear terms of small increments as below

$$\begin{aligned} \begin{pmatrix} \alpha_i \\ \underset{\sim i}{s}^* + \Delta \underset{\sim i}{s}^* \end{pmatrix} &= \sum_{j=1}^{8} k_{ij} \underset{\sim p_i j}{v} - C_{p_i}^{-1} F_{p_i} + \sum_{j=1}^{8} \Delta k_{ij} \underset{\sim p_i j}{v} \\ &= \sum_{j=1}^{8} k_{i-1j} e^{\lambda_{p_{i-1}j} t_{i-1}} \underset{\sim p_{i-1}j}{v} - C_{p_{i-1}}^{-1} F_{p_{i-1}} + \sum_{j=1}^{8} \Delta k_{i-1j} e^{\lambda_{p_{i-1}j} t_{i-1}} \underset{\sim p_{i-1}j}{v} \\ &\quad + \Delta t_{i-1} \sum_{j=1}^{8} k_{i-1j} e^{\lambda_{p_{i-1}j} t_{i-1}} \lambda_{p_{i-1}j} \underset{\sim p_{i-1}j}{v}, \quad 1 \leqslant i \leqslant n. \end{aligned} \tag{17}$$

Initially, a stable period-1 LCO with $n = 4$ can be easily located from the perturbation step. As the bifurcation parameter U^* varies, the LCO may undergo various bifurcations such as symmetry breaking and period doubling, and n may become very large.

To solve Eq. (12) in an efficient way, the following matrix dimension reduction technique is used for large n. This technique is a part of the PI method for non-smooth systems.

3.3. Matrix dimension reduction

Let v_{i0l} and v_{ijl} ($1 \leqslant i \leqslant n$ and $1 \leqslant j, l \leqslant 8$) be the lth component of $C_i^{-1} F_i$ and $\underset{\sim ij}{v}$, respectively. Define vectors K_i, ΔK_i, L_{ilm}, $L_{ilm}^{(\lambda)}$ and matrices M_{im}, $M_{im}^{(\lambda)}$ as

$$\begin{aligned} K_i &= (k_{i1}\, k_{i2} \cdots k_{i8})^{\mathrm{T}}, \quad \Delta K_i = (\Delta k_{i1}\, \Delta k_{i2} \cdots \Delta k_{i8})^{\mathrm{T}}, \\ L_{ilm} &= (e^{\lambda_{i1} t_m} v_{i1l}\, e^{\lambda_{i2} t_m} v_{i2l} \cdots e^{\lambda_{i8} t_m} v_{i8l}), \\ L_{ilm}^{(\lambda)} &= (\lambda_{i1} e^{\lambda_{i1} t_m} v_{i1l} \lambda_{i2} e^{\lambda_{i2} t_m} v_{i2l} \cdots \lambda_{i8} e^{\lambda_{i8} t_m} v_{i8l}), \\ M_{im} &= (e^{\lambda_{i1} t_m} \underset{\sim i1}{v}\; e^{\lambda_{i2} t_m} \underset{\sim i2}{v} \cdots e^{\lambda_{i8} t_m} \underset{\sim i8}{v}) \end{aligned}$$

and

$$M_{im}^{(\lambda)} = (\lambda_{i1} e^{\lambda_{i1} t_m} \underset{\sim i1}{v}\; \lambda_{i2} e^{\lambda_{i2} t_m} \underset{\sim i2}{v} \cdots \lambda_{i8} e^{\lambda_{i8} t_m} \underset{\sim i8}{v}).$$

With the above definitions, it follows from Eq. (17) that

$$\alpha_i = v_{i-101} + \sum_{j=1}^{8} k_{i-1j} e^{\lambda_{p_{i-1}j} t_{i-1}} v_{p_{i-1}j1} + \sum_{j=1}^{8} \Delta k_{i-1j} e^{\lambda_{p_{i-1}j} t_{i-1}} v_{p_{i-1}j1}$$
$$+ \Delta t_{i-1} \sum_{j=1}^{8} k_{i-1j} e^{\lambda_{p_{i-1}j} t_{i-1}} v_{p_{i-1}j1}$$
$$\Longrightarrow \Delta t_{i-1} = (\alpha_i - v_{i-101} - L_{p_{i-1}1i-1} K_{i-1} - L_{p_{i-1}1i-1} \Delta K_{i-1}) / L^{(\lambda)}_{p_{i-1}1i-1} K_{i-1} \tag{18}$$

and

$$M_{p_{i-1}i-1} \Delta K_{i-1} - M_{p_i 0} \Delta K_i + M^{(\lambda)}_{p_{i-1}i-1} K_{i-1} \Delta t_{i-1} = R_i, \tag{19}$$

where $R_i = \sum_{j=1}^{8} k_{ij} \underset{\sim}{v}_{p_i j} - C_{p_i}^{-1} F_{p_i} - \sum_{j=1}^{8} k_{i-1j} e^{\lambda_{p_{i-1}j} t_{i-1}} \underset{\sim}{v}_{p_{i-1}j} + C_{p_{i-1}}^{-1} F_{p_{i-1}}$. Substituting Eq. (18) into Eq. (19), we obtain

$$S_{i-1} \Delta K_{i-1} = M_{p_i 0} \Delta K_i + T_i \tag{20a}$$

$$\Longrightarrow \Delta K_{i-1} = S_{i-1}^{-1} M_{p_i 0} S_i^{-1} M_{p_{i+1}0} \cdots S_{n-1}^{-1} M_{p_n 0} \Delta K_n$$
$$+ \sum_{j=i}^{n} S_{i-1}^{-1} M_{p_i 0} S_i^{-1} M_{p_{i+1}0} \cdots S_{j-1}^{-1} T_j, \tag{20b}$$

where

$$S_{i-1} = M_{p_{i-1}i-1} - M^{(\lambda)}_{p_{i-1}i-1} K_{i-1} L_{p_{i-1}1i-1} / L^{(\lambda)}_{p_{i-1}1i-1} K_{i-1}$$

and

$$T_i = R_i + \frac{M^{(\lambda)}_{p_{i-1}i-1} K_{i-1}}{L^{(\lambda)}_{p_{i-1}1i-1} K_{i-1}} (v_{i-101} + L_{p_{i-1}1i-1} K_{i-1} - \alpha_i).$$

For $i = 1$ in Eq. (20a), $\Delta K_n = S_n^{-1}(M_{p_1 0} \Delta K_1 + T_1)$. Substituting the above equation into Eq. (20b) and let $i = 2$, we obtain

$$\Delta K_1 = (I_8 - S_1^{-1} M_{p_2 0} S_2^{-1} M_{p_3 0} \cdots S_{n-1}^{-1} M_{p_n 0} S_n^{-1} M_{p_1 0})^{-1}$$
$$\times \sum_{j=1}^{n} S_1^{-1} M_{p_2 0} S_2^{-1} M_{p_3 0} \cdots S_{j-1}^{-1} T_j, \tag{21}$$

where I_8 is the 8×8 identity matrix and $S_0 = S_n$.

Once ΔK_1 is found from Eq. (21), the other unknowns ΔK_i, Δs_i and Δt_i can be obtained from Eqs. (20b), (18) and (17), respectively. Therefore, solving the system of $16n$ equations in Eq. (17) involves only the computation of 8×8 matrices. The values of k_{ij}, $\underset{\sim}{s}_i^*$ and t_i are updated by adding the original values and the corresponding incremental values. The iteration process continues until the residue terms are less than a desired degree of accuracy. The entire incremental process proceeds by adding the ΔU^* increment to the converged value of U^* using the previous solution as the initial approximation until a new converged solution is obtained.

4. Stability of LCO

Let Z_{q_i} ($q_i \in \{1, 2\}$) be the switching subspace in which X_i lies. In the present incremental method, a LCO is considered as an equilibrium point of a Poincaré map on Z_{p_1}. For a general LCO with n switching points X_i ($1 \leqslant i \leqslant n$), a Poincaré map Π_1 on Z_{p_1} can be defined by

$$X' = \Pi_1(X), \tag{22}$$

where $X' \in Z_{q_1}$ is obtained from the solution of motion (12) with initial point X and X_1 is an equilibrium point of Π_1. We note that α_1 in $X_1 = (\alpha_1 \ \underset{\sim 1}{s}^*)^{\mathrm{T}}$ remains unchanged when the bifurcation parameter U^* varies. Let Σ be the seven-dimensional subspace of Z_{p_1} defined as

$$\Sigma = \left\{ \underset{\sim 1}{s} \in \Sigma \mid X = \begin{pmatrix} \alpha_1 \\ \underset{\sim 1}{s} \end{pmatrix} \in Z_{q_1} \right\}.$$

To simplify the computation, we defined the reduced Poincaré map on Σ from Eq. (22) as

$$\underset{\sim 1}{s}' = \Pi(\underset{\sim 1}{s}), \tag{23}$$

where $X = (\alpha_1 \ \underset{\sim 1}{s})^{\mathrm{T}}$, $X' = (\alpha_1 \ \underset{\sim 1}{s}')^{\mathrm{T}}$ and $\underset{\sim 1}{s}$ in $X_1 = (\alpha_1 \ \underset{\sim 1}{s}^*)$ is an equilibrium point of Π. The stability of a LCO is determined by the eigenvalues of the first derivative of the reduced Poincaré map Π evaluated at $\underset{\sim 1}{s}^*$. Bifurcations occur when the linearized map is degenerate, i.e. at least one eigenvalue has unit modulus [22,23]. The first derivative $D\Pi$ is given by $D\Pi = \partial\Pi/\partial \underset{\sim 1}{s}$ which can be computed directly by using implicit differentiation. For a general LCO with n switching points, it follows from the chain rule that

$$D\Pi = \frac{\partial \Pi}{\partial \underset{\sim n}{s}} \frac{\partial \underset{\sim n}{s}}{\partial \underset{\sim n-1}{s}} \cdots \frac{\partial \underset{\sim 2}{s}}{\partial \underset{\sim 1}{s}}. \tag{24}$$

To compute $\partial \underset{\sim i+1}{s} / \partial \underset{\sim i}{s}$ for $1 \leqslant i \leqslant n$ and noting that $\partial \underset{\sim n+1}{s} / \partial \underset{\sim n}{s} = \partial \Pi / \partial \underset{\sim n}{s}$, we partially differentiate both sides of $X_i = \underset{\sim i}{r}(0)$ from Eq. (13) with respect to s_{il} where s_{il} is the lth entry of $\underset{\sim i}{s}$ and obtain

$$\begin{aligned} \frac{\partial X_i}{\partial s_{il}} = \underset{\sim l+1}{e} &= \sum_{j=1}^{8} \frac{\partial k_{p_i j}}{\partial s_{il}} \underset{\sim p_i j}{v} = M_{p_i 0} \frac{\partial K_{p_i}}{\partial s_{il}} \\ \Longrightarrow \frac{\partial K_{p_i}}{\partial s_{il}} &= M_{p_i 0}^{-1} \underset{\sim l+1}{e} \end{aligned}$$

where $1 \leqslant l \leqslant 7$ and $\underset{\sim l+1}{e}$ is the 8×1 unit vector with one at the $(l+1)$th entry and zero elsewhere. Partially differentiating both sides of $X_{i+1} = \underset{\sim i}{r}(t_i)$ from Eq. (13) with respect to s_{il}, we further obtain

$$\begin{aligned} 0 &= \sum_{j=1}^{8} \left[\frac{\partial k_{p_i j}}{\partial s_{il}} v_{p_i j 1} \mathrm{e}^{\lambda_{p_i j} t_i} + k_{p_i j} v_{p_i j 1} \lambda_{p_i j} \mathrm{e}^{\lambda_{p_i j} t_i} \frac{\partial t_i}{\partial s_{il}} \right] \\ &= L_{p_i 1 i} \frac{\partial K_{p_i}}{\partial s_{il}} + L_{p_i 1 i}^{(\lambda)} K_{p_i} \frac{\partial t_i}{\partial s_{il}} \\ \Longrightarrow \frac{\partial t_i}{\partial s_{il}} &= \frac{-L_{p_i 1 i} M_{p_i 0}^{-1} \underset{\sim l+1}{e}}{L_{p_i 1 i}^{(\lambda)} K_{p_i}} \end{aligned}$$

and

$$\begin{aligned} \frac{\partial s_{i+1 m}}{\partial s_{il}} &= \sum_{j=1}^{8} \left[\frac{\partial k_{p_i j}}{\partial s_{il}} v_{p_i j m+1} \mathrm{e}^{\lambda_{p_i j} t_i} + k_{p_i j} v_{p_i j m+1} \lambda_{p_i j} \mathrm{e}^{\lambda p_i j t_i} \frac{\partial t_i}{\partial s_{il}} \right] \\ &= L_{p_i m+1 i} \frac{\partial K_{p_i}}{\partial s_{il}} + L_{p_i m+1 i}^{(\lambda)} K_{p_i} \frac{\partial t_i}{\partial s_{il}} \\ \Longrightarrow \frac{\partial s_{i+1 m}}{\partial s_{il}} &= \left(L_{p_i m+1 i} - \frac{L_{p_i m+1 i}^{(\lambda)} K_{p_i} L_{p_i 1 i}}{L_{p_i 1 i}^{(\lambda)} K_{p_i}} \right) M_{p_i 0}^{-1} \underset{\sim l+1}{e} \end{aligned} \tag{25}$$

where $1 \leqslant m \leqslant 7$. The stability of a LCO can be determined by evaluating the eigenvalues of $D\Pi$ from Eqs. (24) and (25). If all the eigenvalues lie inside the unit circle C, the equilibrium point $\underset{\sim}{s}{}_1^*$ is stable. As the bifurcation parameter is varied, eigenvalues may pass through C, at which point a bifurcation occurs. If an eigenvalue crosses C at $+1$, a symmetry-breaking or saddle-node bifurcation may occur. It is a period-doubling (PD) bifurcation if an eigenvalue crosses C at -1. Other than ± 1, the bifurcation is called *Neimark–Sacker bifurcation.*

5. Results and discussions

To compare with the previous results in Refs. [7,11], the system parameters under consideration are chosen as

$$\mu = 100, \quad a_h = -1/2, \quad x_\alpha = 1/4, \quad \zeta_\xi = \zeta_\alpha = 0, \quad r_\alpha = 0.5 \quad \text{and} \quad \bar{\omega} = 0.2.$$

The nonlinear restoring force $M(x_1)$ is given by Eq. (4) with

$$M_0 = 0, \quad M_f = 0, \quad \delta = 0.5^\circ \quad \text{and} \quad \alpha_f = 0.25^\circ,$$

and the plunge is linear with $G(x_3) = x_3$. The linear flutter speed $U_L^* = 6.2851$ is determined by solving the aeroelastic system for $M_0 = \delta = \alpha_f = 0$. For $U^* > U_L^*$, some of the eigenvalues in regions R_1, R_2 and R_3 have positive real parts. Thus, the solution is divergent. As U^* decreases below U_L^*, the real parts of all eigenvalues of the system in R_1 and R_3 are negative, but some eigenvalues in R_2 may have positive real parts. Hence, for $U^* < U_L^*$, the aeroelastic system admits various nonlinear behaviours.

To obtain an initial guess from the perturbation step, we observe that, for U^* slightly less that $U_L^* = 6.2851$, a pair of complex eigenvalues of the system (matrix B) in R_2 have positive real part. These two eigenvalues become pure imaginary at $U_1^* \simeq 0.1691 U_L^*$ where $\lambda = \pm\omega i = \pm 0.1651\text{i}$ and the corresponding eigenvectors $\underset{\sim 1}{u} + \text{i}\underset{\sim 2}{u}$ up to a scalar are given by $\underset{\sim 1}{u} = (-0.1250\ 0.0001\ 0.1245\ 0.0048\ -0.1971\ -0.3206\ 0.0292\ 0.2776)^{\text{T}}$ and $\underset{\sim 2}{u} = (-0.0006\ -0.0206\ -0.0291\ 0.0206\ 0.7028\ 0.1746\ -0.7462\ -0.2499)^{\text{T}}$. It follows from Eq. (11) that $p_1 = 2.0000$ and $p_2 = 0.0096$. We further observe that, in Eq. (5b), $F_2 = 0$ and matrix B has a zero eigenvalue, i.e. $\det(B) = 0$. From Eqs. (8) and (9a,b), $\underset{\sim 0}{u}$ is simply the eigenvector of B with zero eigenvalue such that $u_{01} = \alpha_f + \delta/2 = 0.5$. It is, therefore, given by $\underset{\sim 0}{u} = (0.5\ 0\ -0.2825\ 0\ 10.9890\ 1.6667\ -6.2096\ -0.9418)^{\text{T}}$. The travelling time between the two switching point is $T/2 = \pi/\omega = 19.0284$. With this initial solution, Eq. (24) is employed to construct the continuation curves in U^*.

For the incremental step, we choose the size of the increment ΔU^* to be 0.01. We observe that an unstable symmetric LCO is born at U_1^*. The continuation curve of the symmetric LCO is given in Fig. 6. Initially, one eigenvalue of the first derivative $D\Pi$ is outside the unit circle. As U^* decreases to $U_2^* = 0.1310 U_L^*$, a saddle-node bifurcation occurs where an eigenvalue leaves the unit circle at $+1$. As U^* increases again and $\max(\alpha)$ increases, the LCO encounters a Neimark–Sacker (Secondary Hopf) bifurcation at $U_3^* = 0.1353 U_L^*$ (label 3) where a pair of eigenvalues enter the unit circle at points other than ± 1. The LCO is stable until a subcritical symmetry-breaking bifurcation occurs at $U_4^* = 0.2194 U_L^*$ (label 4) where an eigenvalue leaves the unit circle at $+1$. At this value, the stable symmetric LCO merges with two other unstable asymmetric LCOs and becomes unstable. A LCO is asymmetric if it is not symmetric. As U^* increases further, another subcritical symmetry-breaking bifurcation occurs at $U_5^* = 0.6880 U_L^*$ (label 5) and the LCO becomes stable again. The amplitude continues to grow without a bound as U^* tends to U_L^*. The initial switching point X_1, period and stability of the stable symmetric LCO at $U^* = 0.7 U_L^*$ are given in Table 1. A phase portrait of this LCO is shown in Fig. 7 and is compared to the result obtained by using the fourth-order Runge–Kutta method. They are in good agreement.

Next, we consider the emanating curve arisen from one of the asymmetric LCOs born at U_4^* as depicted in Fig. 8. On the emanating curve, four PD bifurcations are found at $U_6^* = 0.2132 U_L^*$ (label 6), $U_7^* = 0.21216 U_L^*$ (label 7), $U_9^* = 0.2511 U_L^*$ (label 9) and $U_{10}^* = 0.5280 U_L^*$ (label 10); one Neimark–Sacker bifurcation at $U_8^* = 0.1968 U_L^*$ (label 8); two saddle-node bifurcations at $U_{11}^* = 0.1950 U_L^*$ and $U_{12}^* = 0.7575 U_L^*$. We note that the

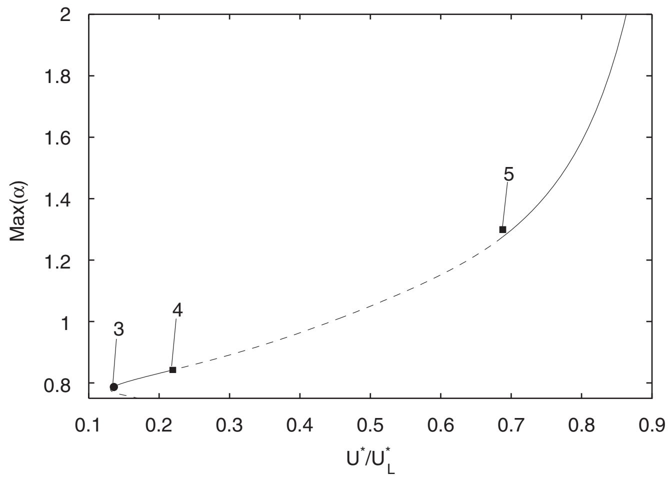

Fig. 6. Continuation curve of symmetric LCO; •, Neimark–Sacker bifurcation; ■, symmetry-breaking bifurcation.

Table 1
The initial switching point, period and stability of symmetric LCO at $U^* = 0.7U_L^*$

Type of motion: p-1 (symmetric)	Period: 72.0471
Initial switching point: (0.25 0.0462 $-$5.5757 0.1435 4.4438 0.2507 $-$124.6945 $-$19.8591)	
Floquet multipliers: 0.7494, 0.1231, $0.0443 \pm 0.0183i$, 0.0377, 0, 0	

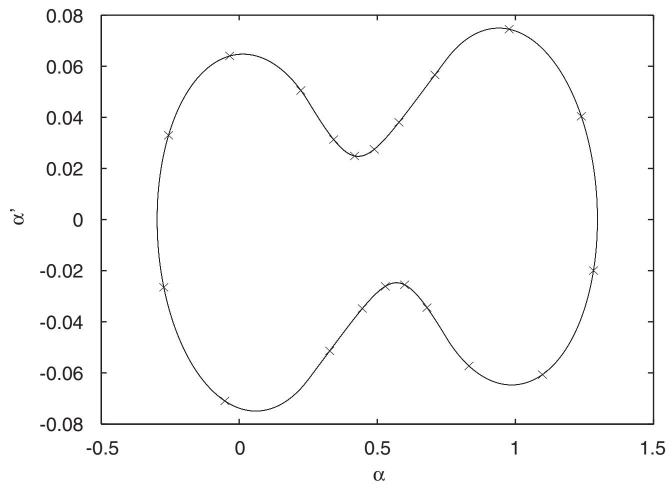

Fig. 7. Symmetric LCO at $U^* = 0.7U_L^*$: ——, Runge–Kutta method; ×, perturbation-incremental method.

period-1 LCO is stable in the ranges (U_8^*, U_9^*), (U_{10}^*, U_{12}^*) and all of these LCOs contain harmonics. A phase portrait of the stable asymmetric LCO at $U^* = 0.7U_L^*$, which coexists with that of Fig. 7, is shown in Fig. 9. The initial switching point, period and stability of this LCO are given in Table 2.

The bifurcation results in Figs. 6 and 8 give insight into the numerical results obtained in Refs. [7,11]. The bifurcation diagrams in Fig. 11 of Ref. [7] and Fig. 6 of Ref. [11] are obtained from trajectories with a fixed initial point when U^* varies. It was pointed out in Ref. [11] that, in Fig. 6, there is a small reduction in amplitude for pitch when the bifurcation parameter is increased to cross $U^* = 0.732U_L^*$ and the solution

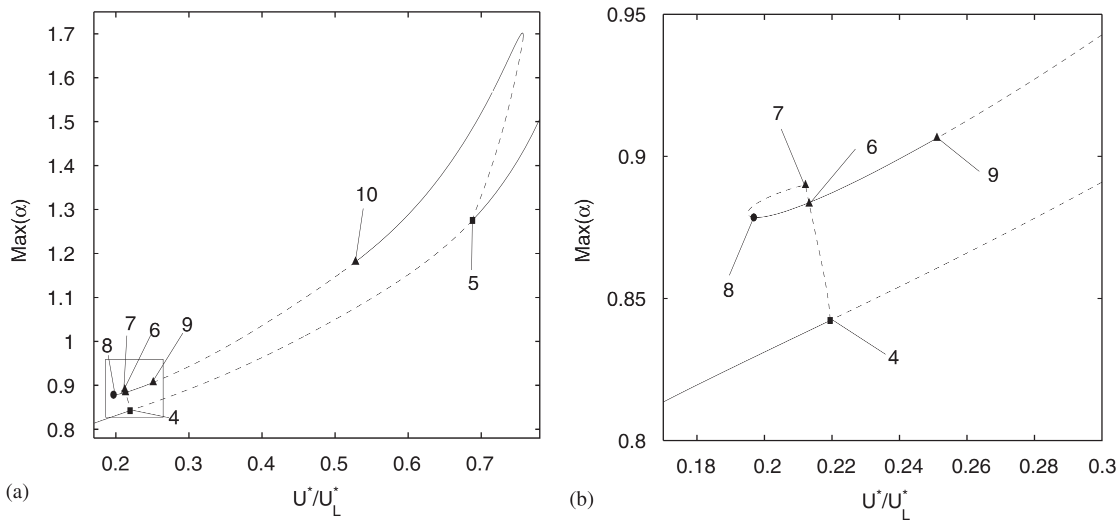

Fig. 8. (a) Continuation curve of one of the asymmetric LCO. (b) Enlarged diagram near $U^* = 0.2U_L^*$: •, Neimark–Sacker bifurcation; ▲, period-doubling bifurcation; ■, symmetry-breaking bifurcation.

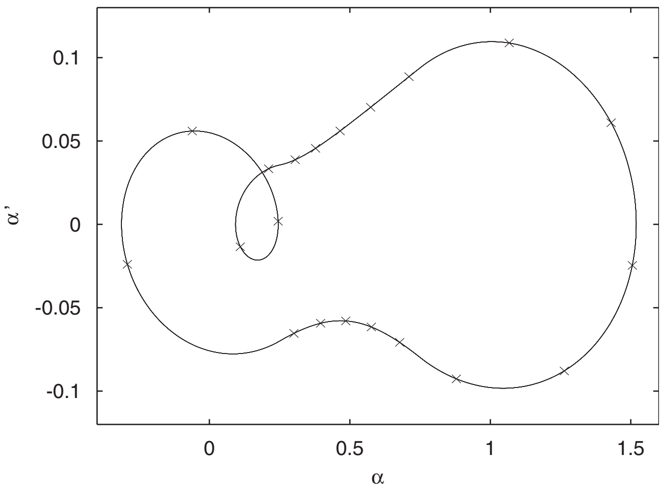

Fig. 9. One of the asymmetric LCOs at $U^* = 0.7U_L^*$: —, Runge–Kutta method; ×, perturbation-incremental method.

Table 2
The initial switching point, period and stability of one of the asymmetric LCO at $U^* = 0.7U_L^*$

Type of motion: p-1-h (asymmetric)	Period: 81.9851
Initial switching point: (0.25 0.0356 −2.8777 0.1719 3.9468 0.5756 −103.5019 −11.5272)	
Floquet multipliers: $-0.1944 \pm 0.1286i$, 0.0495, 0.0240, 0.0353, 0, 0	

becomes a simple period-1 LCO. From Figs. 6 and 8 above, the reason for the reduction is that the trajectory jumps from one of the coexisting asymmetric LCO to the symmetric LCO. Furthermore, the discontinuity of the bifurcation curve in Fig. 6 of Ref. [11] for the range $0.53U_L^* \leqslant U^* \leqslant 0.732U_L^*$ is due to the jump of the trajectories between the two coexisting asymmetric LCOs.

The emanating branches from the PD bifurcations of Fig. 8 at U_6^* (label 6) and U_9^* (label 9) are shown in Figs. 10(a) and (b), respectively. On the emanating branch ($B1$) from U_6^*, two more PD bifurcations are found at $U_{11}^* = 0.2132U_L^*$ (label 11) and $U_{12}^* = 0.21217U_L^*$ (label 12). Emanating branches of further PD bifurcations are shown in Fig. 11 where branch Bn ($n = 1, 2, 3$) contains period-2^n LCOs. The emanating branches suggest a sequence of PD bifurcations leading to chaos. However, this phenomenon is not observed in Fig. 6 of Ref. [11] as the LCOs on these branches are all unstable. On the emanating branch ($B1$) from U_9^* (see Fig. 10(b)), three saddle-node bifurcations ($U_{13}^* = 0.2484U_L^*$, $U_{16}^* = 0.5548U_L^*$, $U_{17}^* = 0.4879U_L^*$) and two PD bifurcations ($U_{14}^* = 0.2489U_L^*$ (label 14), $U_{15}^* = 0.5546U_L^*$ (label 15)) are found. The period-2 LCOs on the curve segments (U_{13}^*, U_{14}^*), (U_{17}^*, U_{10}^*) and (U_{15}^*, U_{16}^*) are stable. Emanating branches of further PD bifurcations are shown in Figs. 12(a)–(c) where branch Bn ($n = 1, 2, 3$) contains period-2^n LCOs. In Fig. 12(a), branches $B2$ and $B3$ are visually indistinguishable. In Figs. 12(b) and (c), two sequences of stable PD bifurcations leading to chaos are

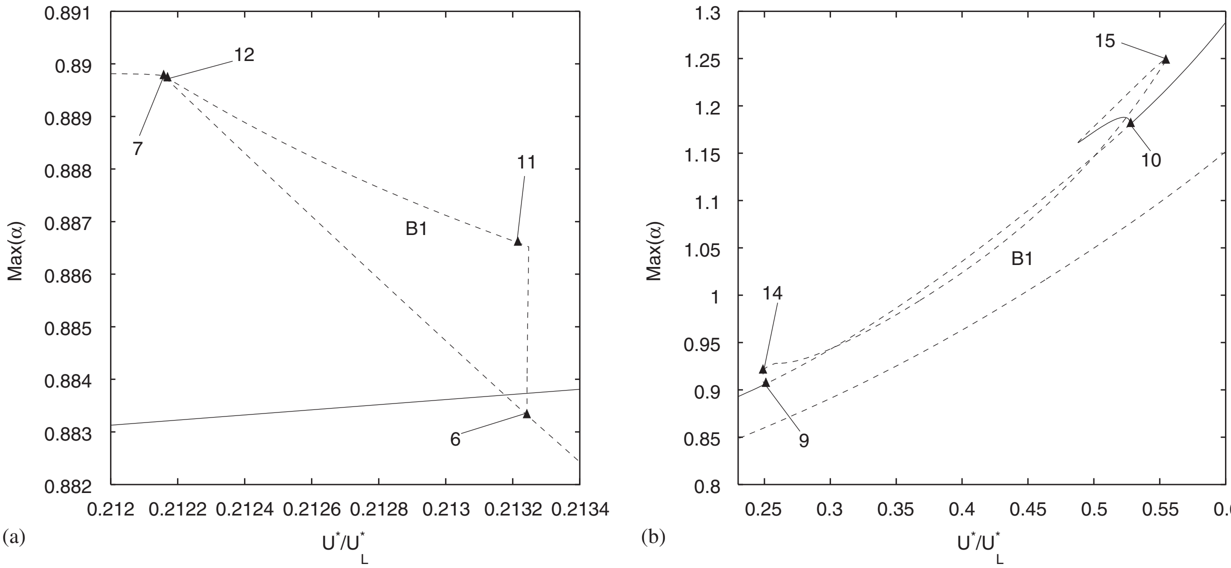

Fig. 10. Emanating branches from the period-doubling bifurcations of Fig. 8: ▲, period-doubling bifurcation.

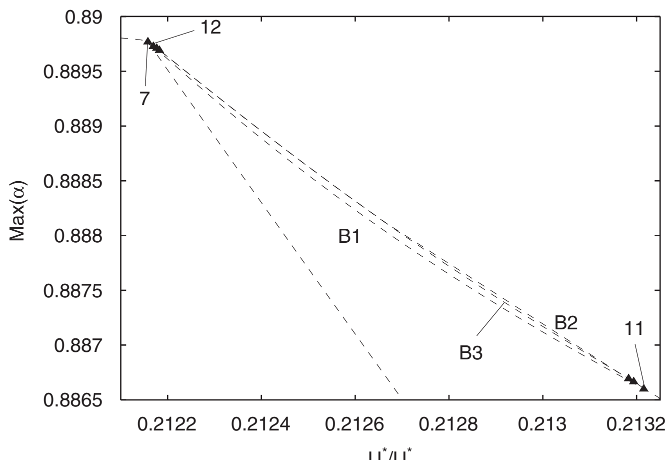

Fig. 11. Emanating branches of PD bifurcation arisen from U_6^*: ▲, period-doubling bifurcation.

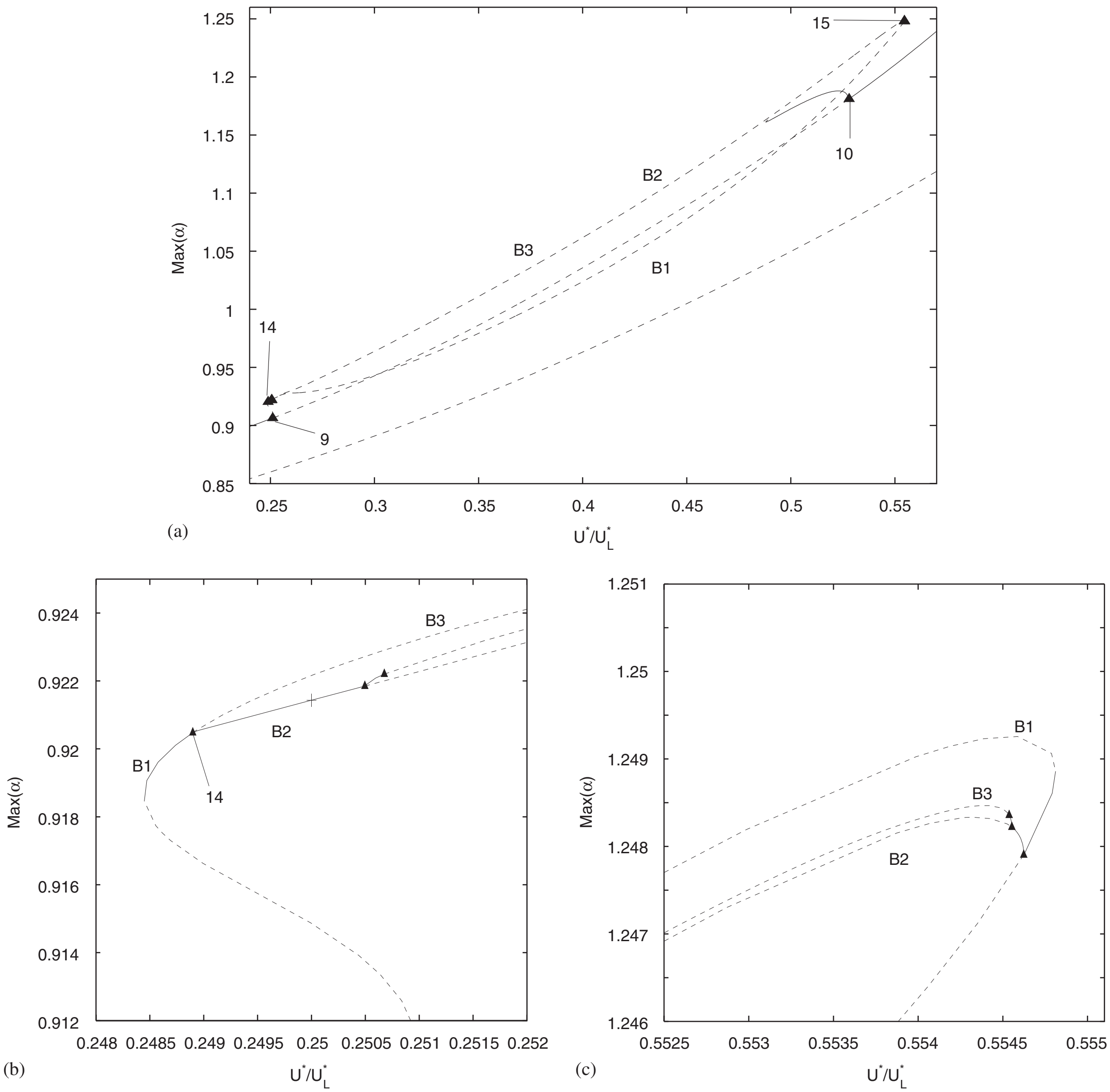

Fig. 12. Emanating branches of PD bifurcations arisen from U_9^*: ▲, period-doubling bifurcation.

observed. Since the bifurcation values between consecutive PD bifurcations are very small, it is expected that full chaos will be developed soon after the occurrence of PD bifurcations at around $U^* = 0.25U_L^*$ and $0.55U_L^*$. The former case was reported in Ref. [11]. A phase portrait of the stable period-4-h LCO at $U^* = 0.25U_L^*$ (label 16) on branch $B2$ of Fig. 12(b) is shown in Fig. 13. The initial switching point, period and stability of this LCO are given in Table 3.

In Fig. 7 of Ref. [11], period-2-h LCOs are found between $0.325U_L^* \leqslant U^* \leqslant 0.466U_L^*$ by the PT method. However, these LCOs are not contained in any of the continuation curves we constructed previously. To construct the continuation curve relating to these LCOs, we first obtain the LCO at, say $U^* = 0.4U_L^*$ by using the Runge–Kutta method. The phase portrait and information of this LCO are given in Fig. 14 and Table 4, respectively. With this p-2-h LCO as the initial solution, we apply the incremental step and obtain the

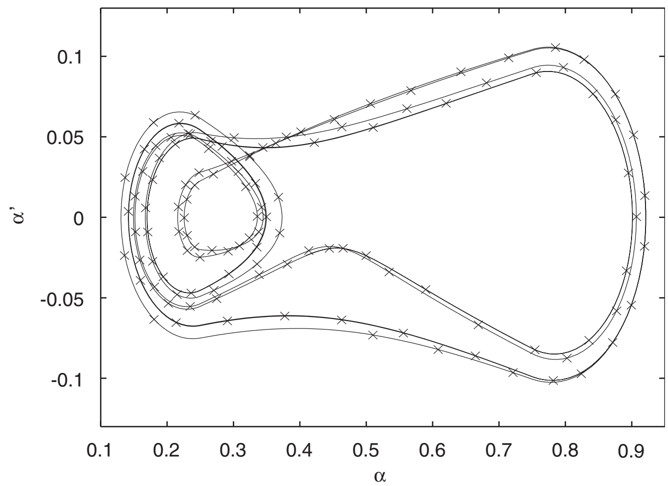

Fig. 13. Period-4-h LCO at $U^* = 0.25U_L^*$ on branch $B2$ of Fig. 12(b): ——, Runge–Kutta method; ×, perturbation-incremental method.

Table 3
The initial switching point, period and stability of the period-4-h LCO at $U^* = 0.25U_L^*$ on branch $B2$ of Fig. 12(b)

Type of motion: p-4-h	Period: 171.3142
Initial switching point: (0.25 0.0616 −0.9719 −0.0437 9.1392 0.8084 −10.6221 −2.6389)	
Floquet multipliers: $-0.2016 \pm 0.6601i$, 0.0004, 0.0004, 0.0002, 0, 0	

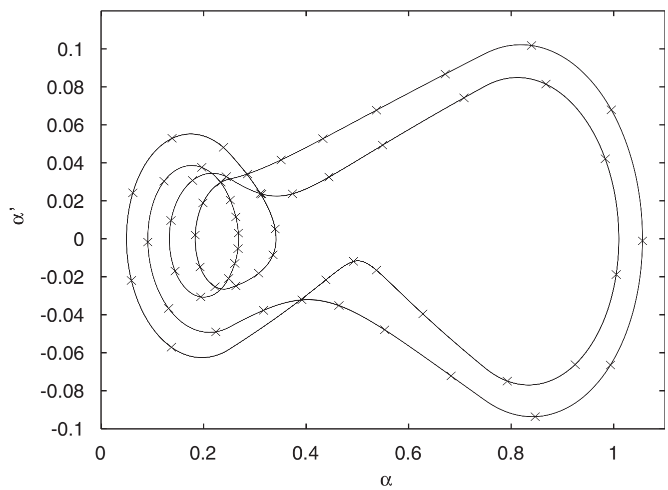

Fig. 14. Period-2-h LCO at $U^* = 0.4U_L^*$: ——, Runge–Kutta method; ×, perturbation-incremental method.

Table 4
The initial switching point, period and stability of the period-2-h LCO at $U^* = 0.4U_L^*$

Type of motion: p-2-h	Period: 120.3980
Initial switching point: (0.25 0.0451 −2.2714 0.0319 8.2265 0.5330 −36.8109 −7.6077)	
Floquet multipliers: −0.3429, 0.0889, −0.0175, 0.0042, 0.0047, 0, 0	

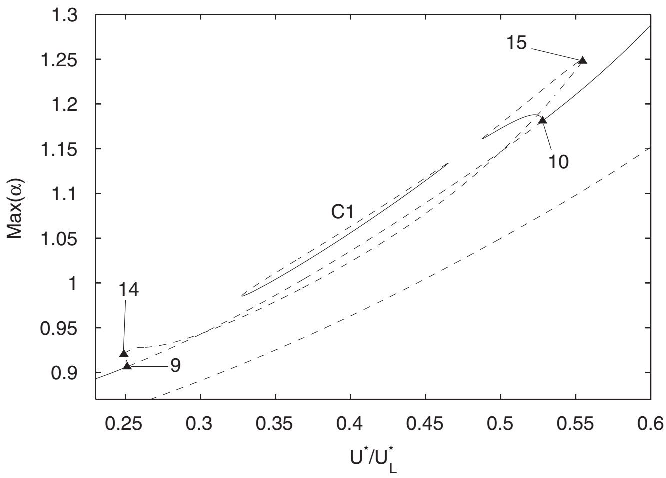

Fig. 15. A separated continuation curve $C1$ which forms a closed loop: ▲, period-doubling bifurcation.

continuation curve $C1$ as depicted in Fig. 15. It is interesting to note that this curve forms a closed loop. From Fig. 7 of Ref. [11], it seems that, as U^* increases, the p-2-h LCO passes through the chaotic region and becomes period-1 at $U^* = 0.53U_L^*$ where a large drop with a factor of two in the period occurs. However, from Fig. 15, the p-2-h LCO in fact disappears at $U^* = 0.4652U_L^*$ due to a saddle-node bifurcation. Therefore, the results obtained from the PI method give us a clearer and more accurate picture about the global bifurcations of the freeplay model as this method is able to capture the unstable solutions while the PT method is not capable of doing so.

6. Conclusion

A perturbation-incremental (PI) method has been developed to investigate the dynamic response of a self-excited two-degree of freedom aeroelastic system with structural nonlinearity represented by a freeplay stiffness. The PI method overcomes the main disadvantage of the harmonic balance (HB) method in that the first derivative of an approximate LCO obtained by the present method is piecewise continuous which agrees qualitatively with the exact solution while that obtained by the HB method is differentiable, thus providing an accurate prediction of the switching points where the changes in linear subdomains occur. The present method is also able to compute unstable LCOs and gives a full picture of the global bifurcation.

In comparing with the PT method, the advantage of the PI method is that it is capable of capturing the unstable LCOs and is able to perform continuation while the PT method is not. However, the PI method cannot include the initial condition in the analysis while the PT method does show the effect of the initial condition.

The continuation curves in Figs. 6, 8, 10, 12 and 15 obtained by the PI method provide insight into the previous bifurcation results found in Refs. [7,11]. For instance, in Fig. 6 of Ref. [11], a sudden reduction of pitch amplitude at $U^* = 0.732U_L^*$ is due to a change of the trajectory from one of the coexisting asymmetric LCOs to the symmetric LCO and the discontinuity of the bifurcation curve in the range $0.53U_L^* \leqslant U^* \leqslant 0.732U_L^*$ is a result of the switching of trajectories between the two coexisting asymmetric LCOs.

In the incremental step, a matrix dimension reduction technique is presented to reduce a system of $16n$ equations with the same number of unknowns to the computation of iterative matrices with dimension 8×8. Although this technique reduces greatly the computational time, it works as long as U^* is used as the bifurcation parameter since the eigenvalues and eigenvectors of matrices A and B in Eq. (6) can be determined before the iterations. However, in the vicinity of a saddle-node bifurcation where U^* can no longer be used as the bifurcation parameter, U^* and thus the eigenvalues, eigenvectors of matrices A, B become unknowns whose values have to be constantly updated in each iterative process. In that case, the dimension of the iterative matrices will be much larger than 8×8 although the dimension technique can still be applied.

Neimark–Sacker (Secondary Hopf) bifurcation is detected in Figs. 6 and 8. The continuation of such bifurcation may also be made possible by the PI method. We recall that a LCO can be considered as an equilibrium point of a Poincaré map in a switching subspace. Then, a quasi-periodic solution can be regarded as an invariant curve in the switching subspace. Previous techniques developed in Refs. [12–15] for the computation of limit cycles can be employed to compute invariant curves as they have similar features. This will be pursued in future research.

From the illustrative examples presented in this paper, it is clearly demonstrated that analytic predictions from the PI method are in excellent agreement with those resulting from the PT method and a numerical time-integration scheme. Although the investigation is concentrated on an aeroelastic system with a structural freeplay nonlinearity in the pitch degree of freedom, the analysis can readily be extended to include nonlinearities in both degree of freedom and to hysteresis models.

Acknowledgements

This work was supported by the strategic research Grant 7001557 of the City University of Hong Kong. The valuable and constructive comments from the anonymous referees are highly appreciated.

Appendix A. Definitions of coefficients

$$
\begin{aligned}
a_{21} &= j(-d_5c_0 + c_5d_0), \quad a_{41} = j(d_5c_1 - c_5d_1),\\
a_{22} &= j(-d_3c_0 + c_3d_0), \quad a_{42} = j(d_3c_1 - c_3d_1),\\
a_{23} &= j(-d_4c_0 + c_4d_0), \quad a_{43} = j(d_4c_1 - c_4d_1),\\
a_{24} &= j(-d_2c_0 + c_2d_0), \quad a_{44} = j(d_2c_1 - c_2d_1),\\
a_{25} &= j(-d_6c_0 + c_6d_0), \quad a_{45} = j(d_6c_1 - c_6d_1),\\
a_{26} &= j(-d_7c_0 + c_7d_0), \quad a_{46} = j(d_7c_1 - c_7d_1),\\
a_{27} &= j(-d_8c_0 + c_8d_0), \quad a_{47} = j(d_8c_1 - c_8d_1),\\
a_{28} &= j(-d_9c_0 + c_9d_0), \quad a_{48} = j(d_9c_1 - c_9d_1),
\end{aligned}
$$

where j, $c_i\,(i = 0, 1, 2, \ldots, 9)$ and $d_i\,(i = 0, 1, 2, \ldots, 9)$ are defined as

$$
\begin{aligned}
&j = \frac{1}{c_0d_1 - c_1d_0},\\
&c_0 = 1 + \frac{1}{\mu}, \quad c_1 = x_\alpha - \frac{a_h}{\mu},\\
&c_2 = \frac{2}{\mu}(1 - \psi_1 - \psi_2), \quad c_3 = \frac{1}{\mu}(1 + (1 - 2a_h)(1 - \psi_1 - \psi_2)),\\
&c_4 = \frac{2}{\mu}(\varepsilon_1\psi_1 + \varepsilon_2\psi_2), \quad c_5 = \frac{2}{\mu}\left(1 - \psi_1 - \psi_2 + \left(\frac{1}{2} - a_h\right)(\varepsilon_1\psi_1 + \varepsilon_2\psi_2)\right),\\
&c_6 = \frac{2}{\mu}\varepsilon_1\psi_1\left(1 - \varepsilon_1\left(\frac{1}{2} - a_h\right)\right), \quad c_7 = \frac{2}{\mu}\varepsilon_2\psi_2\left(1 - \varepsilon_2\left(\frac{1}{2} - a_h\right)\right),\\
&c_8 = -\frac{2}{\mu}\varepsilon_1^2\psi_1, \quad c_9 = -\frac{2}{\mu}\varepsilon_2^2\psi_2,\\
&d_0 = \frac{x_\alpha}{r_\alpha^2} - \frac{a_h}{\mu r_\alpha^2}, \quad d_1 = 1 + \frac{1 + 8a_h^2}{8\mu r_\alpha^2},
\end{aligned}
$$

$$d_2 = -\frac{1+2a_h}{\mu r_\alpha^2}(1-\psi_1-\psi_2),$$
$$d_3 = \frac{1-2a_h}{2\mu r_\alpha^2} - \frac{(1+2a_h)(1-2a_h)(1-\psi_1-\psi_2)}{2\mu r_\alpha^2},$$
$$d_4 = -\frac{1+2a_h}{\mu r_\alpha^2}(\varepsilon_1\psi_1+\varepsilon_2\psi_2),$$
$$d_5 = -\frac{1+2a_h}{\mu r_\alpha^2}(1-\psi_1-\psi_2) - \frac{(1+2a_h)(1-2a_h)(\psi_1\varepsilon_1-\psi_2\varepsilon_2)}{2\mu r_\alpha^2},$$
$$d_6 = -\frac{(1+2a_h)\psi_1\varepsilon_1}{\mu r_\alpha^2}\left(1-\varepsilon_1\left(\frac{1}{2}-a_h\right)\right),$$
$$d_7 = -\frac{(1+2a_h)\psi_2\varepsilon_2}{\mu r_\alpha^2}\left(1-\varepsilon_2\left(\frac{1}{2}-a_h\right)\right),$$
$$d_8 = \frac{(1+2a_h)\psi_1\varepsilon_1^2}{\mu r_\alpha^2}, \quad d_9 = \frac{(1+2a_h)\psi_2\varepsilon_2^2}{\mu r_\alpha^2},$$
$$\psi_1 = 0.165, \quad \psi_2 = 0.335, \quad \varepsilon_1 = 0.0455, \quad \varepsilon_2 = 0.3.$$

Appendix B. Definitions of matrices and vectors

$$A_1 = \begin{pmatrix} 0 & 1 & 0 & 0 \\ a_{21} - jc_0\left(\frac{1}{U^*}\right)^2 & a_{22} & a_{23} + jd_0\beta\left(\frac{\bar{\omega}}{U^*}\right)^2 & a_{24} \\ 0 & 0 & 0 & 1 \\ a_{41} + jc_1\left(\frac{1}{U^*}\right)^2 & a_{42} & a_{43} - jd_1\beta\left(\frac{\bar{\omega}}{U^*}\right)^2 & a_{44} \end{pmatrix},$$

$$A_2 = \begin{pmatrix} 0 & 0 & 0 & 0 \\ a_{25} & a_{26} & a_{27} & a_{28} \\ 0 & 0 & 0 & 0 \\ a_{45} & a_{46} & a_{47} & a_{48} \end{pmatrix}, \quad A_3 = \begin{pmatrix} 1 & 0 & 0 & 0 \\ 1 & 0 & 0 & 0 \\ 0 & 0 & 1 & 0 \\ 0 & 0 & 1 & 0 \end{pmatrix}, \quad A_4 = \begin{pmatrix} -\varepsilon_1 & 0 & 0 & 0 \\ 0 & -\varepsilon_2 & 0 & 0 \\ 0 & 0 & -\varepsilon_1 & 0 \\ 0 & 0 & 0 & -\varepsilon_2 \end{pmatrix},$$

$$B_1 = \begin{pmatrix} 0 & 1 & 0 & 0 \\ a_{21} - jc_0M_f\left(\frac{1}{U^*}\right)^2 & a_{22} & a_{23} + jd_0\beta\left(\frac{\bar{\omega}}{U^*}\right)^2 & a_{24} \\ 0 & 0 & 0 & 1 \\ a_{41} + jc_1M_f\left(\frac{1}{U^*}\right)^2 & a_{42} & a_{43} - jd_1\beta\left(\frac{\bar{\omega}}{U^*}\right)^2 & a_{44} \end{pmatrix}, F = \begin{pmatrix} 0 \\ -jc_0\left(\frac{1}{U^*}\right)^2 \\ 0 \\ jc_1\left(\frac{1}{U^*}\right)^2 \\ 0 \\ 0 \\ 0 \\ 0 \end{pmatrix}.$$

References

[1] D.S. Woolston, H.L. Runyan, R.E. Andrews, An investigation of effects of certain types of structural nonlinearities on wing and control surface flutter, *Journal of Aeronautical Sciences* 24 (1) (1957) 57–63.

[2] S.F. Shen, An approximate analysis of nonlinear flutter problems, *Journal of Aerospace Sciences* 26 (1) (1959) 25–32.

[3] S.C. McIntosh Jr., R.E. Reed Jr., W.P. Rodden, Experimental and theoretical study of nonlinear flutter, *Journal of Aircraft* 18 (1981) 1057–1063.

[4] Z.C. Yang, L.C. Zhao, Analysis of limit cycle flutter of an airfoil in incompressible flow, *Journal of Sound and Vibration* 123 (1990) 1–13.

[5] A.J. Hauenstein, R.M. Laurenson, W. Eversman, G. Galecki, I. Qumei, A.K. Amos, Chaotic response of aerosurfaces with structural nonlinearities, *Proceedings of the AIAA/ASME/ASCE/AHS/ASC 33rd Structures, Structural Dynamics, and Materials Conference, Part 4 Structural Dynamics II* (*Dallas, TX*), AIAA, Washington, DC, 1992, pp. 2367–2375.

[6] S.J. Price, H. Alighanbari, B.H.K. Lee, The aeroelastic response of a two-dimensional airfoil with bilinear and cubic structural nonlinearities, *Proceedings of the AIAA/ASME/ASCE/AHS/ASC 35th Structures, Structural Dynamics, and Materials Conference*, (Hilton Head, SC), AIAA, Washington, DC, 1994, pp. 1771–1780.

[7] S.J. Price, B.H.K. Lee, H. Alighanbari, Post instability behavior of a two-dimensional airfoil with a structural nonlinearity, *Journal of Aircraft* 31 (6) (1994) 1395–1401.

[8] D.M. Tang, E.H. Dowell, Flutter and stall response of a helicopter blade with structural nonlinearity, *Journal of Aircraft* 29 (5) (1992) 953–960.

[9] S.H. Kim, I. Lee, Aeroelastic analysis of a flexible airfoil with a freeplay nonlinearity, *Journal of Sound and Vibration* 193 (4) (1996) 823–846.

[10] S.L. Lau, W.S. Zhang, Nonlinear vibrations of piecewise-linear systems by incremental harmonic balance method, *Journal of Applied Mechanics* 59 (1992) 153–160.

[11] L. Liu, Y.S. Wong, B.H.K. Lee, Nonlinear aeroelastic analysis using the point transformation method—part 1: freeplay model, *Journal of Sound and Vibration* 253 (2) (2002) 447–469.

[12] H.S.Y. Chan, K.W. Chung, Z. Xu, A perturbation-incremental method for strongly nonlinear oscillators, *International Journal of Nonlinear Mechanics* 31 (1996) 59–72.

[13] K.W. Chung, C.L. Chan, Z. Xu, G.M. Mahmoud, A perturbation-incremental method for strongly nonlinear autonomous oscillators with many degrees of freedom, *Nonlinear Dynamics* 28 (2002) 243–259.

[14] K.W. Chung, C.L. Chan, J. Xu, An efficient method for switching branches of period-doubling bifurcations of strongly nonlinear autonomous oscillators with many degrees of freedom, *Journal of Sound and Vibration* 267 (2003) 787–808.

[15] K.W. Chung, C.L. Chan, J. Xu, A perturbation-incremental method for delay differential equations, *International Journal of Bifurcation and Chaos* 16 (8) (2006) (to appear).

[16] Y.C. Fung, *An Introduction to the Theory of Aeroelasticity*, Dover, New York, 1993.

[17] B.H.K. Lee, S.J. Price, Y.S. Wong, Nonlinear aeroelastic analysis of airfoils: bifurcation and chaos, *Progress in Aerospace Sciences* 35 (1999) 205–334.

[18] R.T. Jones, The unsteady lift of a wing of finite aspect ratio, *NACA Report* 681 (1940).

[19] K.W. Chung, Y.B. He, B.H.K. Lee, Bifurcation analysis of a two-degree-of-freedom aeroelastic system with hysteresis structural nonlinearity by a perturbation-incremental method, in preparation.

[20] E. Freire, E. Ponce, F. Rodrigo, F. Torres, Bifurcation sets of continuous piecewise-linear system with two zeros, *International Journal of Bifurcation and Chaos* 8 (11) (1998) 2073–2097.

[21] E. Freire, E. Ponce, J. Ros, Limit cycle bifurcation from centre in symmetric piecewise-linear systems, *International Journal of Bifurcation and Chaos* 9 (5) (1999) 895–907.

[22] J. Guckenheimer, P. Holmes, *Nonlinear Oscillations, Dynamical systems, and Bifurcations of Vector Fields*, Springer, New York, 1983.

[23] A.H. Nayfeh, B. Balachandran, *Applied Nonlinear Dynamics: Analytical, Computational, and Experimental Methods*, Wiley, New York, 1995.